Technical note: Studying Li-metaborate fluxes and extraction protocols with a new, fully automated *in situ* cosmogenic ^{14}C processing system at PRIME Lab

5 Nathaniel Lifton[1,2], Jim Wilson[3], Allie Koester[1]

[1]Department of Earth, Atmospheric, and Planetary Sciences, Purdue University, 550 Stadium Mall Drive, West Lafayette, Indiana, 47907, USA.
[2]Department of Physics and Astronomy and Purdue Rare Isotope Measurement Laboratory (PRIME Lab), Purdue
10 University, 525 Northwestern Avenue, West Lafayette, Indiana, 47907, USA.
[3]Aeon Laboratories, LLC, 5835 North Genematas Drive, Tucson, Arizona, 85704, USA.

Correspondence to: Nathaniel Lifton (nlifton@purdue.edu)

Abstract. Extraction procedures for *in situ* cosmogenic [14]C (*in situ* [14]C) from quartz require quantitative isotopic yields while maintaining scrupulous isolation from atmospheric/organic [14]C. These time- and labor-intensive
15 procedures are ripe for automation; unfortunately, our original automated *in situ* [14]C extraction and purification systems, reconfigured and retrofitted from our original systems at the University of Arizona, proved less reliable than hoped. We therefore installed a fully automated stainless-steel system (except for specific borosilicate glass or fused-silica components) incorporating more reliable valves and improved actuator designs, along with a more robust liquid nitrogen distribution system. As with earlier versions, the new system uses a degassed Li-metaborate
20 ($LiBO_2$) flux to dissolve the quartz sample in an ultra-high-purity oxygen atmosphere, after a lower-temperature combustion step to remove atmospheric/organic [14]C.

We compared single-use high-purity Al_2O_3 vs. reusable 90%Pt/10%Rh (Pt/Rh) sample combustion boats. The Pt/Rh boats heat more evenly than the Al_2O_3, reducing procedural blank levels and variability for a given $LiBO_2$ flux. This lower blank variability also allowed us to trace progressively increasing blanks to specific batches of fluxes from our
25 original manufacturer. Switching to a new manufacturer returned our blanks to consistently low levels on the order of $(3.4 \pm 0.9) \times 10^4$ [14]C atoms.

We also analyzed the CRONUS-A intercomparison material to investigate sensitivity of extracted ^{14}C concentrations to the temperature and duration of the combustion and extraction steps. Results indicate that 1-hr combustion steps at either 500 or 600°C yield results consistent with the consensus value of Jull et al. (2015), while 2 hr at 600°C
30 results in loss of ca. 9% of the high-temperature ^{14}C inventory. Results for 3 hr extractions at temperatures ranging from 1050°C to 1120°C and 4.5 hr at 1000°C yielded similar results that agreed with the nominal value as well as with published results from most laboratories. On the other hand, an extraction for 3 hr at 1000°C was judged to be incomplete due to a significantly lower measured concentration. Based on these results, our preferred technique is now combustion for 1 hr at 500°C followed by a 3 hr extraction at 1050°C. Initial analyses of the CoQtz-N
35 intercomparison material at our lab yielded concentrations ca. 60% less than those of CRONUS-A, but more analyses of this material from this and other labs are clearly needed to establish a consensus value.

Deleted: low-temperature combustion/high-temperature extraction…
Deleted: systematics
Deleted: quartz

1 Introduction

Extracting in situ cosmogenic [14]C (*in situ* [14]C) from quartz is challenging in that minute quantities of ^{14}C must be extracted and purified from quartz samples while preventing contamination by ubiquitous atmospheric/organic [14]C. These extraction and purification procedures are time-consuming and labor-intensive when done manually – as such they are attractive targets for automation. Lifton et al. (2015) presented results from the initial automated *in situ* [14]C extraction and purification systems at the Purdue Rare Isotope Measurement Laboratory (PRIME Lab), reconfigured and retrofitted from our original glass systems at the University of Arizona. As hoped, the automation of key components of our *in situ* [14]C lab indeed led to increased throughput and reproducibility. While the overall timeline of the extraction, purification, and graphitization was still ca. 3 days, a single person was able to operate both automated extraction systems, the automated purification system, and the manual graphitization system simultaneously, boosting sample throughput significantly over the purely manual systems.

These automated systems comprised two independent extraction systems and a separate CO_2 purification system. A separate system for converting CO_2 to graphite was not automated. This required custom design and implementation of equipment to automate three key aspects of the systems: servo-based valve actuators, temperature control for cryogenic gas purification, and liquid nitrogen (LN) transfer. While these automated systems improved throughput over our original purely manual systems, they also required manual transfer of sample gas between separate extraction, purification, and (manual) graphitization systems.

However, in terms of overall reliability of operation, the limitations of retrofitting our original designs ultimately became apparent. For example, the glass high-vacuum valves are not precision components – no two are precisely the same. The valve actuators thus had to adapt to differences in resistance to motion arising from variations in valve stem and valve bore diameters, as well as to different lengths of travel to adequately seat each valve. As originally designed, the valve actuators accommodated these variations well, but the mechanical settings at which each operated properly tended to creep over time, such that sometimes during active processes individual valves might not indicate that they are closed or open, or might indicate a closed position but not be seated properly and allow leakage across the valve. Without actively checking on the system status when this happened, the sample gas could be pumped away by accident, or a process could be interrupted (which could lead to system damage).

Similarly, the LN distribution system in that system was ultimately problematic. LN was transferred from a pressurized 200 L supply dewar through insulated Teflon tubing to fill dewars on various cold traps. Filling and emptying of individual dewars was controlled using LN level sensors comprising three resistors in series, positioned with resistors at empty, nominal, and full levels within each dewar. During the processes, certain cold traps needed to be alternately filled and emptied. Dewars stationed on those traps were emptied using a small shop vacuum cleaner via a drain manifold fitted with cryogenic solenoid valves. Particularly at times of high humidity (not as much of an issue in arid Arizona as in Indiana), ice condensation in those dewars could cause the drain tubing to clog and interrupt the process sequence. Also, sometimes when a particular dewar was filled and emptied multiple times in a process sequence, the resistor string would not register the proper voltage during a fill cycle to trigger shutoff of LN flow, and the dewar would overflow continuously unless an operator was present to close the main

supply dewar valve manually. Thus, although sample throughput and repeatability was considerably improved over manual operation, system reliability was not at the point where one could generally leave a system in unattended operation.

80 We thus recently purchased and installed a customized Carbon Extraction and Graphitization (CEGS) system from Aeon Laboratories, LLC, similar to that of Goehring et al. (2019) at Tulane University. The largely stainless-steel system (except for specific sections requiring borosilicate glass or fused-silica components) incorporates more reliable valves and improved actuator designs compared to our original system, as well as a robust and efficient liquid nitrogen distribution system (see Goehring et al. (2019) for additional details). The new system, controlled by

85 a flexible and extensible modular software package written in C#, follows a similar procedure to that of Lifton et al. (2015), using a degassed Li-metaborate ($LiBO_2$) flux to dissolve the quartz sample in a Research Purity (RP) O_2 atmosphere. In addition, all sections of the new system are connected, so that one can extract all evolved carbon species as CO_2 from a quartz sample, purify and precisely measure the resulting gas yield, and convert the CO_2 to graphite for AMS analysis – all without human intervention. Below we describe key differences relative to the

90 system of Goehring et al. (2019), then present baseline results from the now fully operational system, including procedural blanks and analyses of established intercomparison materials, for both our original single-use high-purity aluminum oxide and new reusable 90%Pt/10%Rh sample boats.

2 Purdue CEGS design and operation

The Purdue CEGS (PCEGS) comprises three main modules: two extraction modules and a

95 collection/purification/graphitization module (main CEGS module) (Fig. 1), following the general design of Goehring et al. (2019) but with an additional extraction module. However, the PCEGS differs from the latter system in two key aspects. First, the two PCEGS extraction modules (Tube Furnace 1 [TF1] and Tube Furnace 2 [TF2]) are connected in parallel, each accommodating a high-temperature resistance furnace with a mullite furnace tube and evacuated by separate vacuum systems distinct from the main CEGS vacuum system (Fig. 1). On the other hand, the

100 Goehring et al. (2019) system comprises one tube furnace in series with the CEGS, evacuated by a single vacuum system. Our design allows each PCEGS extraction module to run processes independently of those controlled by the other modules, enabling increased flexibility in system operations. The other key difference is that condensable gases evolved on the PCEGS during an extraction procedure in either furnace are trapped in a compact borosilicate glass coil trap held at LN temperature (-196°C) instead of the variable temperature trap (VTT) used for this purpose

105 on the Goehring et al. (2019) system (Figs. 1, 2). The compact coil trap (ca. 3.5 cm diameter x ca. 10 cm tall) derives from our previous larger coil trap designs (e.g., Lifton et al., 2001; Pigati et al., 2010; Lifton et al., 2015), which consistently demonstrated quantitative trapping of minute CO_2 quantities from O_2 carrier gas. This compact design ensures similarly reliable CO_2 trapping through a 9 mm o.d. x 7 mm i.d. inlet downtube, delivering process gases directly to the base of the trap before passing through a constriction connecting the downtube to a 6 mm o.d. x

110 4 mm i.d. coiled section and outlet tube (Fig. 2). The total length of the trap submerged in LN when operating is ca. 55 cm (ca. 5 cm of the downtube and the ca. 50 cm coil).

Other than incorporating a U-shaped secondary oxidation furnace (9 mm o.d. x 7 mm i.d. filled with 2 mm quartz beads, held at ca. 900°C) from the Lifton et al. (2015) system instead of an inline granular quartz oxidation furnace of the Goehring et al. (2019) design, the rest of the PCEGS utilizes similar hardware to that of the latter. However, our six-reactor graphitization manifold is configured in front of the main purification and measurement process path to achieve a shorter footprint than the linear configuration of the Tulane system (Fig. 1), allowing the first extraction module and the CEGS module to fit onto our existing lab frame and benchtop.

We implement a two-day extraction procedure with the PCEGS similar to those of Lifton et al. (2015) and Goehring et al. (2019), utilizing a lithium metaborate ($LiBO_2$) flux to dissolve the quartz and release the *in situ* [14]C at 1100°C (Table 1). The first day's procedures involve degassing the $LiBO_2$ flux and preparing the purified quartz for extraction, while the second day is the extraction/purification/graphitization procedure. Once started, the Day 1 $LiBO_2$ degassing process operates on the selected extraction module (either TF1 or TF2) completely independently of the main CEGS module. The Day 2 process, on the other hand, requires control from the main CEGS module to allow sample collection, purification, measurement, dilution, and graphitization. In practical terms, we execute a Day 1 process on one extraction module, then the next day start a Day 1 process on the second extraction module. The Day 2 process for the first extraction module can then be run without interruption from the main CEGS module. The Day 1 and Day 2 processes are then subsequently cycled between the two extraction modules. This comfortably allows for PCEGS throughput of 4-5 samples per week.

On Day 1, a quartz sample is pretreated with 50% (v:v) HNO_3:18 MΩ water for at least 90 min in an ultrasonic bath, rinsed thoroughly in 18 MΩ water, then dried in a vacuum oven overnight. A sample boat (either single-use high-purity Al_2O_3 or reusable 90%Pt-10%Rh) containing ca. 20 g of pre-fused $LiBO_2$ beads (melting point 845°C) is placed inside a flame-cleaned fused-silica sleeve in the mullite furnace tube (with borosilicate glass o-ring ball joint end seals), using flame-cleaned implements. The 24-inch-long (60.96 cm) fused-silica sleeve (replaced after every sample) extends beyond the furnace hot zone, protecting the furnace tube from $LiBO_2$ vapors that evolve from the fused sample at high temperature. The aggressively reactive vapors etch the interior of the sleeve within the hot zone of the furnace, instead of the furnace tube itself (Fig. 3). To minimize intrusion of atmospheric CO_2 or other contaminant gases into the furnace tube each time it is opened, the tube is first backfilled with Research Purity He (99.9999%) to 20 torr above ambient atmospheric pressure. The He is then slowly bled through the tube while open to atmosphere. Once closed again, the furnace tube is evacuated to <5 x 10^{-3} torr, isolated, and 50 torr of RP O_2 is subsequently added. The furnace is then heated to the extraction temperature (typically 1100°C) for 1 hour while O_2 is bled through with a mass flow controller and automated metering valve to maintain the tube pressure and to flush out any evolved contaminants to the vacuum pump. The tube is then cooled and evacuated overnight.

On Day 2, after backfilling the tube with He as before, the boat with degassed $LiBO_2$ is removed (again with flame-cleaned implements) to a HEPA-filtered laminar flow bench. Approximately 5 g of the pretreated quartz sample is evenly distributed over the now-solid $LiBO_2$ in the boat and the boat+sample is returned to the furnace, evacuated to <5 x 10^{-3} torr, isolated, and 50 torr RP O_2 is added again. The sample is then heated to 500°C for one hour to combust and remove atmospheric/organic contaminants, while bleeding O_2 across the sample as before and

Deleted: quartz

Deleted:

Deleted: quartz

Deleted: prevent

Deleted: s

Deleted: from entering

Deleted: when

Deleted: approximately

exhausting to the vacuum system. After that hour, the 500°C tube furnace is evacuated to <5 x 10^{-3} torr. Subsequently, 50 torr of RP O_2 is admitted into the tube furnace and the sample/flux is heated to 1100°C and held at the high temperature for three hours to dissolve the quartz and release any trapped carbon species. During extraction

160   the O_2 pressure in the tube typically rises to ca. 60 torr.

After the extraction procedure completes, the evolved gases are bled with RP O_2 through the secondary oxidation furnace to ensure any carbon species released during extraction are completely oxidized to CO_2 before collection in the compact coil trap cooled with LN. During this step, the tube pressure at the end of the extraction step is maintained during the bleed (to prevent excess $LiBO_2$ vaporization) while the furnace cools to <800°C (to ensure

165   complete melt solidification), before shutting off additional O_2 inflow and slowly evacuating all tube gases through the secondary furnace and coil trap. The condensed gases are then transferred to the purification section to remove water, halogens, and nitrogen and sulfur oxides. The gas is transferred cryogenically with LN first into the variable temperature trap (VTT) and the incondensable gases are evacuated. The VTT is then warmed to -145°C for 10 minutes to remove sulfur oxides, water, and other contaminant gases from the sample CO_2. The evolved CO_2 is then

170   passed through a Cu mesh/Ag wool trap held at 600 °C (removes nitrogen oxide, halogen, and sulfur oxide contaminants) and frozen with LN into the volumetric measurement chamber (MC) (Fig. 1). The CO_2 yield is then measured manometrically as equivalent mass of C (μg), and typically diluted to ca. 300 μg C with ^{14}C-free CO_2. A ca. 9 μg C split (ca. 3% of the total C mass) is collected in a pre-evacuated Exetainer® vial for stable C isotopic analysis offline, and the remaining sample is transferred cryogenically to one of the six graphite reactors (Fig. 1).

175   The sample then undergoes hydrogen reduction (with Research Purity H_2 – 99.9999%) to filamentous C (graphite) on an Fe catalyst, with water trapped by $Mg(ClO_4)_2$ (Southon, 2007; Santos et al., 2004). Procedural background samples are run after approximately every 7-10 unknown samples, using identical procedures without adding quartz.

Finally, the graphite is packed into an Al cathode for ^{14}C measurement by Accelerator Mass Spectrometry (AMS) at PRIME Lab. Sample ^{14}C/^{13}C ratios are measured relative to Oxalic Acid II (NIST-4990C). Stable carbon isotopic

180   ratios were measured at the University of California at Davis Stable Isotope Facility (stableisotopefacility.ucdavis.edu) using isotope ratio mass spectrometry (Lifton et al., 2015). Measured *in situ* ^{14}C concentrations are calculated from the resulting ^{14}C/C$_{total}$ after subtracting representative procedural background ^{14}C values, following Hippe and Lifton (2014). Measurement uncertainties are presented at the 1σ level unless otherwise noted.

185   **3 Initial Experiments**

Once the PCEGS was operational, we began to characterize its performance in terms of procedural blank (background) values as well as measurements of intercomparison materials such as CRONUS-A (Jull et al., 2015). We also characterized the mass-dependence of graphitization blanks. Since publication of Lifton et al. (2001), we and other labs using $LiBO_2$ for extraction (e.g., Goehring et al., 2019; Lamp et al., 2019; Fülöp et al., 2010) had used

190   single-use high purity sintered Al_2O_3 combustion boats for our flux + samples. On the other hand, laboratories that implemented flux-free *in situ* ^{14}C extractions have either used Pt (e.g., Hippe et al., 2009, 2013; Lupker et al., 2019) or fused-silica vessels (Fülöp et al., 2015, 2019). The labs using flux-free processes typically report blanks on the

Deleted: , while t

Deleted:

Deleted: quartz

order of $1\text{-}3\text{x}10^4$ ^{14}C atoms (e.g., Lupker et al., 2019; Fülöp et al., 2019), while the labs using flux-based extractions have reported blanks on the order of $1\text{-}2\text{x}10^5$ ^{14}C atoms (e.g., Lifton et al., 2015; Goehring et al., 2019; Lamp et al., 2019). Goehring et al. (2019) deduced that the differences in ^{14}C backgrounds between the flux and flux-free extraction systems lay at least in part with the sintered Al_2O_3 boats reacting with the flux to release small and variable amounts of persistent contaminant ^{14}C during the extraction process. They described assessing boats of alternate construction, and reported a promising process blank result of ca. $4\text{x}10^4$ ^{14}C atoms from an initial experiment with a reusable 90%Pt:10%Rh alloy boat.

Our initial PCEGS experiments utilized the single-use Al_2O_3 combustion boats, but in the meantime, we also obtained a set of 90%Pt:10%Rh (hereafter Pt/Rh) combustion boats from Heraeus Precious Metals North America LLC (www.pt-labware.com). We thus compared results using both types of boats, for both blanks and intercomparison samples. The solidified $LiBO_2$+sample melt is cleaned from the Pt/Rh boats between samples by overnight ultrasonication at 40°C in 10% (v:v) reagent grade HNO_3:18 MΩ water in sealed 1L polypropylene bottles, followed by thorough rinsing in 18 MΩ water and drying in a gravity oven.

3.1 Graphitization blanks

The mass-dependence of the PCEGS graphitization blanks was assessed by graphitizing aliquots of ^{14}C-free CO_2 in masses ranging from ca. 50 µg C to 1000 µg C (Table 2). As with previous studies using either Zn or H_2 as the reducing agent for CO_2 to C (e.g., Donahue et al., 1990; Lifton et al., 2001, 2015; Goehring et al., 2019), we observe an inverse relationship between sample mass (in µg C) and the measured $^{14}C/C_{total}$. If one assumes a constant modern contaminant contribution to the graphitization blank from the graphitization reactor, independent of the sample mass, then one would observe an inverse mass dependence of the blank: higher blanks for lower mass samples (e.g., Donahue et al., 1990). This relationship is well-characterized by the equation (adjusted $R^2 = 0.994$)

$$B_g = (1.243 \pm 0.045) \times 10^{-13}\big/_{mass} + (1.301 \pm 0.050) \times 10^{-15} \qquad (1)$$

Correction of the measured sample $^{14}C/C_{total}$ for the graphitization blank $^{14}C/C_{total}$ (B_g) follows Eq. 6 of Donahue et al. (1997).

3.2 Procedural blank comparison

Initial experiments with the new system involved procedural blanks with our original single-use Al_2O_3 boats in concert with measurements of intercomparison materials (Section 3.3). Subsequently, we switched to reusable 90%Pt/10%Rh sample boats, with associated measurements of procedural blanks and intercomparison materials for a range of experimental conditions.

3.2.1 Al_2O_3 boats

The first set of blanks and intercomparison samples processed on the PCEGS with Al_2O_3 boats involved a more aggressive than normal Day 2 combustion step to more thoroughly remove any potential organic C that might remain on the etched sample grains. This was motivated by Nichols and Goehring (2019) who found evidence of

modern ^{14}C contamination by laurylamine used in froth flotation mineral separation techniques that was not removed completely by their original etching procedure. Although we had not observed evidence of this issue with *in situ* [14]C results from our lab, we tested a low-temperature combustion procedure of 2 hr. at 600°C, reasoning that Hippe et al. (2013) utilized a 2 hr. at 700°C combustion step with no apparent demonstrable effects on their results

235   relative to combustions for 1 hr. at 500°C. This more aggressive combustion step was then followed by our normal 1100°C flux fusion for 3 hr.

Initial procedural blank experiments largely utilized TF1, and progressively increased from ca. 6.50×10^4 to 1.03×10^5 ^{14}C atoms with a mean of $(8.79 \pm 1.64) \times 10^4$ [14]C atoms, while a single blank from TF2 yielded ca. 1.14×10^5 ^{14}C atoms (Table 3, Fig. 4). The source of the time-dependent increase was not identified before switching to the

240   Pt/Rh boats, but these values still represent an improvement over blank values presented in Lifton et al. (2015) by ca. 30-70%.

3.2.2 Pt/Rh boats

On switching to the Pt/Rh boats, we also reverted to our original procedure utilizing a 500°C combustion step for 1 hr. It was immediately obvious that the Pt/Rh boats heat much more uniformly than the Al_2O_3, based on dramatic

245   differences in the flux's corrosive effects on the quartz sleeves between the two types of boats (Fig. 3). The sleeves used with the Al_2O_3 boats were corroded mainly above and below the boat, as well as at the ends of the heated zone where the $LiBO_2$ vapor condenses in ca. 5 cm-wide bands (Fig. 3a). The rest of the heated portion of the sleeve is only lightly corroded and remains transparent. However, when using the Pt/Rh boats, the $LiBO_2$ more evenly corrodes the sleeve interior over the entire hot zone length (Fig. 3b). Most of the boat heating likely occurs via

250   conduction from the bottom edges of the boat in contact with the quartz sleeve. It thus appears that the more efficient heat conduction of the metal boats leads to more even and aggressive heating of the flux and sample than in the Al_2O_3 boats. Experiments with the Pt/Rh boats at extraction temperatures of 1000°C and 1050°C resulted in significantly less corrosion of the sleeve than at 1100°C (Fig. 3b).

Initial procedural blanks using the Pt/Rh boats were dramatically lower than those using the Al_2O_3 boats, with much

255   better reproducibility, averaging $(4.08 \pm 0.66) \times 10^4$ [14]C atoms (1σ) (Table 4, Fig. 4). Different combinations of combustion (500°C and 600°C – 1 hr) and extraction temperatures/times (1100°C – 3 hr, 1000°C – 3 hr and 4.5 hr) were investigated as well (Table 4) (corresponding to intercomparison experiments described in Section 3.3), with no significant effect on blank results. This supports the hypothesis of Goehring et al. (2019) that a significant component of Al_2O_3 procedural blanks derived from the sintered ceramic boats themselves. The improved blank

260   reproducibility using the Pt/Rh boats allows us to identify background signals that previously we were unable to resolve. After this initial set of analyses depleted most of the bottle of Ultra-Pure grade $LiBO_2$ (Claisse C-0611-00, Batch C-10001 – "Batch 1"), we switched to a new bottle of Pure grade $LiBO_2$ (Claisse C-0610-00, Batch C-17000-10 – "Batch 2"). We reasoned that Pure and Ultra-Pure grades only differ in metal impurity content – both are pre-fused, spherical beads and thus should be essentially functionally equivalent for our application.

Deleted: 2

Deleted: 3

Deleted: 3

However, subsequent blanks with the new bottle increased in both CO_2 yield (ca. 1.5 µg to ca. 4 µg C-equivalent) and ^{14}C content (ca. (1.51 ± 0.31) x 10^5 ^{14}C atoms) (Table 4, Fig. 4). Although these values were higher than the initial measurements, they were reproducible on both TF1 and TF2, so we continued with normal system operation. Subsequently, though, the CO_2 yields and ^{14}C content inexplicably jumped again to new 'stable' values of ca. 6.6 µg C-equivalent and (2.66 ± 0.07) x 10^5 ^{14}C atoms, respectively, using TF1, with a similar but slightly lower result with TF2. At that point we tested a second bottle of Pure grade $LiBO_2$ (Claisse C-0610-00, Batch C-19000-10 – "Batch 3" – purchased at the same time as Batch C-17000-10) on procedural blanks in TF1 (PCEGS-94) and TF2 (PCEGS-95), with even higher results of (3.21 ± 0.10) x 10^5 and (3.63 ± 0.15) x 10^5 ^{14}C atoms, respectively. The higher blanks from Batch C-19000-10 also exhibited higher CO_2 yields (ca. 8-9.5 µg C-equivalent). In fact, the CO_2 yields from each extraction module tracked the ^{14}C atoms quite linearly for all these experiments, with similar regression fits to each (R^2 values of 0.955 and 0.970 for TF1 and TF2, respectively – Fig. 5)

At that point we paused normal system operations and conducted more basic experiments to try to isolate the source of the increased blanks – was it in the system overall or the $LiBO_2$? Two procedural blanks with everything except for the $LiBO_2$ (boat-sleeve only) – one boat cleaned in 10% v:v HCl, and the other in 10% v:v HNO_3 – both yielded ca. 2.0 x 10^4 ^{14}C atoms. This indicated that the $LiBO_2$ was the source of the high blank, although the nature of that source and why the blank increased with time is unclear. This is particularly puzzling since the low blanks with Pt/Rh boats (compared to the boat-and-sleeve-only blanks) indicate that the degassing step on Day 1 should be effective at minimizing atmospheric CO_2 contamination from the flux.

We then obtained a new bottle of Ultra-Pure grade $LiBO_2$ (Claisse C-0611-00, Batch C-19001-10 – "Batch 4"); two blanks from that bottle from TF2 (PCEGS-98 and 99) yielded values comparable to PCEGS-95 – ca. 3.6-3.7 x 10^5 ^{14}C atoms, and ca. 8-9 µg C-equivalent yields (Fig. 4, Table 4). Finally, we tried a blank with the remainder of the original bottle of Ultra-Pure grade $LiBO_2$ (Claisse C-0611-00, Batch C-10001 – "Batch 1"). This experiment (PCEGS-100) exhibited CO_2 yield and ^{14}C content comparable to our original tests: 2.2 µg C-equivalent and 4.76 ± 1.12 x 10^4 ^{14}C atoms. In consultation with Claisse technical support, we were unable to identify any chemical change in their product or manufacturing process that could have led to the progressively increasing blanks. As such, we identified another vendor, SPEX CertiPrep. We purchased a similar pre-fused Ultra-Pure grade $LiBO_2$ from them (FFB-0000-03, Lot 240920D-2904) and ran a blank on each extraction module. CO_2 yields were comparable to those of the original Claisse Ultra-Pure batch, and ^{14}C contents were slightly improved over that material: ca. 2.5 µg C-equivalent and ca. 3.6 x 10^4 ^{14}C atoms (Table 4, Fig. 4). Subsequent blanks with the new SPEX $LiBO_2$ were generally comparable to or better than those initial measurements, ranging from ca. 2.4 x 10^4 to 5.0 x 10^4 ^{14}C atoms (mean: (3.38 ± 0.92) x 10^4 ^{14}C atoms), and similar to recently published blank measurements from other *in situ* ^{14}C laboratories using Pt sample boats (e.g., Lupker et al., 2019; Goehring et al., 2019) (Table 4, Fig. 4). Regardless of the ultimate cause of the unexplained blank behavior with the more recent bottles of Claisse $LiBO_2$, we are proceeding with the SPEX Ultra-Pure $LiBO_2$ as our preferred flux.

Late in this process we also discovered that the temperature controller for TF2 was miscalibrated at high temperature setpoints, reading 1120°C on an independent Type-S thermocouple probe when set to 1100°C. Independent

measurement of the lower temperatures for the combustion steps in TF2 agreed with the setpoints – only the extraction temperatures exhibited the offset. We subsequently adjusted the setpoint temperatures for extractions to achieve the desired temperature on that furnace (1080°C setpoint for 1100°C actual, and 1035°C setpoint for 1050°C actual). No such problem was observed with TF1. Results from both blanks and intercomparison materials (Section 3.3 below) do not appear to indicate any significant effect from the 20°C excess temperature in the affected TF2 experiments (Figs. 4 and 6, Tables 4 and 5).

3.3 Extraction experiments with intercomparison materials

While we worked to isolate and understand the source(s) of the time-dependent procedural blanks on our new system, we also set out to better understand the effects of different combustion temperatures/durations on the amount of ^{14}C extracted from the well-studied CRONUS-A intercomparison material, derived from Antarctic sandstone bedrock of long exposure duration (Jull et al., 2015). In addition, since the more uniform heating of the Pt/Rh boats rendered the LiBO$_2$ flux more broadly aggressive toward the fused-silica sleeves at 1100°C, we tested whether it would be possible to lower the extraction temperature and still achieve full ^{14}C recovery from CRONUS-A. We also initiated measurements at PRIME Lab of the *in situ* ^{14}C content of the CoQtz-N intercomparison material (e.g., Binnie et al., 2019) using both types of boats. CoQtz-N is derived from a boulder of vein quartz in Namibia, again of long exposure duration (Binnie et al., 2019).

3.3.1 CRONUS-A – Al$_2$O$_3$ boats

Initial experiments with the Al$_2$O$_3$ boats used CRONUS-A to test whether the more aggressive combustion procedure described in Section 3.2.1 (2 hr at 600°C) followed by a 3 hr fusion at 1100°C might affect the measured *in situ* ^{14}C concentrations significantly. Results from both TF1 and TF2 yielded ^{14}C concentrations on the order of 10% below the consensus value for the material and outside the uncertainty band (Table 5, Fig. 6), suggesting diffusive loss of *in situ* ^{14}C during the more aggressive low-temperature combustion step. We thus subsequently abandoned that more aggressive procedure in favor of the original 1 hr at 500°C combustion step of Lifton et al. (2001) (also Section 3.2.2) – results from Lifton et al. (2015) using Al$_2$O$_3$ boats with this original procedure are shown for comparison in Fig. 6.

3.3.2 CRONUS-A – Pt/Rh boats

Our efforts with the Pt/Rh boats largely focused on optimizing extraction temperature and time, again using CRONUS-A as a benchmark (Table 5, Fig. 6). We varied combustion and extraction temperatures/durations, using corresponding background corrections appropriate for the procedures used and allowing for the observed procedural blank time-dependence.

The experiments with extractions for 3 hr at 1100°C and 1120°C, and 4.5 hr at 1000°C (PCEGS-44, 46, 50, 90, 104, 105, 106, 133 – Table 5, Fig. 6) yielded a mean and standard deviation of (7.08 ± 0.17) x 10^5 ^{14}C atoms g^{-1} (1σ). An additional extraction test for 3 hr at 1000°C (PCEGS-47) yielded a ^{14}C concentration about 8% lower than this mean, but still within the nominal range of results in Jull et al. (2015). However, we judge this extraction as likely to

be incomplete as it is outside of the 2σ uncertainty of our mean Pt/Rh CRONUS-A analyses, and as such do not consider this further. Another test with a combustion step of 1 hr at 600°C and a normal 1100°C extraction (PCEGS-50) yielded a result ca. 4% below the mean above using a 500°C combustion temperature but within 2σ of that mean, and still well within the Jull et al. (2015) range. Excluding PCEGS-50 from the mean above does not significantly change the mean nor these conclusions. After discovering the furnace controller miscalibration for TF2, we also tested CRONUS-A results for TF2 at 1100°C (PCEGS-105), and found them indistinguishable from the Pt/Rh mean. Finally, given the less aggressive corrosion of the quartz sleeve from tests at 1050°C (Fig. 3b), we also tested CRONUS-A extraction for 3 hr at 1050°C (PCEGS-106), with results indistinguishable from our overall Pt/Rh mean (Table 5, Fig. 6). We thus have switched to a 3 hr at 1050°C extraction temperature/duration going forward.

Our CRONUS-A results are consistent with the consensus value and range of Jull et al. (2015), $(6.93 \pm 0.44) \times 10^5$ ^{14}C atoms g^{-1}, as well as with the mean of our previous results at PRIME Lab (Lifton et al., 2015): $(6.89 \pm 0.04) \times 10^5$ ^{14}C atoms g^{-1}. In addition, these new results are consistent with recent measurements by Lupker et al. (2019), Fülöp et al. (2019), and Lamp et al. (2019) (Fig. 6). Like those other studies, they also disagree with the CRONUS-A measurements of Goehring et al. (2019), for reasons yet to be determined (Fig. 6).

3.3.3 CoQtz-N

Our three results for the CoQtz-N intercomparison material spanned the period discussed in this work (Table 5). An initial analysis using an Al_2O_3 boat and the more aggressive 2 hr combustion at 600°C returned a lower concentration $(2.48 \pm 0.06) \times 10^5$ ^{14}C atoms g^{-1} than the two Pt/Rh experiments at 500°C/1100°C (TF1) and 500°C/1120°C (TF2), which agree within 1σ measurement uncertainties and yield a mean value of $(2.62 \pm 0.04) \times 10^5$ ^{14}C atoms g^{-1}. Interestingly, the Al_2O_3 result with the more aggressive combustion step is only about 5% lower than the Pt/Rh mean CoQtz-N result (uncertainties overlap at 2σ), vs. 9% lower than the nominal value for the Al_2O_3 analyses of CRONUS-A. The source of this difference is not clear, but likely reflects intrinsic differences in diffusive properties of the quartz from each sample.

We only found one other study in which *in situ* ^{14}C had been measured in CoQtz-N (Schiffer et al., 2020), but that study provides incomplete experimental details and only a plot of concentrations vs. quartz mass without any tabulated data. The four measured values presented for 1 g of CoQtz-N appear to span concentrations ca. 3×10^5 to over 4×10^5 ^{14}C atoms g^{-1} – well above our measured values. The source of this discrepancy merits further investigation but currently is difficult to evaluate without complete experimental details.

4 Conclusions

This study details key characteristics of and procedures in use for the new *in situ* ^{14}C extraction system at PRIME Lab (PCEGS), and presents results of initial testing of procedural blanks and intercomparison materials. We compare results using the original single-use Al_2O_3 sample boats employed since Lifton et al. (2001) with those from a new set of reusable 90%Pt/10%Rh alloy sample boats.

Deleted: 4

Deleted: 4

385 It is clear from these experiments that the reusable Pt/Rh boats provide distinct advantages over the Al_2O_3 boats, supporting suggestions of Goehring et al. (2019). First, the Pt/Rh boats appear to heat much more aggressively than the sintered Al_2O_3 ceramic boats, likely leading to more uniform heating of the contents. The Pt/Rh boats also appear to reduce or eliminate a significant component of the blank variability associated with the sintered ceramics, perhaps associated with small amounts of atmospheric carbon potentially incorporated into the ceramics during

390 manufacture. Taken together, the aggressive uniform heating and purity of the Pt/Rh alloy allow for improved analytical reproducibility, allowing robust identification of systematic influences on background signals that we were previously unable to resolve with the Al_2O_3 boats.

Using the Pt/Rh boats, we demonstrated that time-dependent increases in procedural blanks were tied directly to specific batches of $LiBO_2$ fluxes manufactured by Claisse. The time-dependence did not appear to reflect flux

395 purity, but rather some presently unknown characteristic of the Claisse fluxes appears to have changed since the original batch we used for our early experiments. Subsequent analyses with $LiBO_2$ from an alternate supplier, SPEX CertiPrep, yielded consistently low procedural blanks on the order of $(3.4 \pm 0.9) \times 10^4$ ^{14}C atoms, and we have switched to that flux going forward.

We also analyzed two intercomparison materials as part of our initial experiments, to confirm compatibility with

400 earlier results from this lab as well as from others. Using both Al_2O_3 and Pt/Rh boats, we focused mainly on CRONUS-A, but also made initial measurements for our laboratory of the newer CoQtz-N intercomparison material. We first tested CRONUS-A in Al_2O_3 boats using a more aggressive combustion procedure than typically used (2 hr at 600°C vs. 1 hr at 500°C) and found significantly lower ^{14}C concentrations from the high-temperature extraction relative to the nominal value of Jull et al. (2015), likely due to diffusive loss during the more aggressive low-

405 temperature step. Abandoning that aggressive procedure in favor of the shorter 500°C combustion, and switching to the Pt/Rh boats, we then explored various time-temperature combinations for the high-temperature extraction step with CRONUS-A. Results for 3 hr extractions at temperatures ranging from 1050°C to 1120°C and 4.5 hr at 1000°C yielded similar results, in agreement with the consensus value as well as with published results from most laboratories, including those using our previous extraction system (Lifton et al., 2015). On the other hand, an

410 extraction for 3 hr at 1000°C yielded a significantly lower concentration than the other analyses in this study, suggesting incomplete extraction for those conditions. Based on these results, our preferred technique is now combustion for 1 hr at 500°C followed by a 3 hr extraction at 1050°C.

The initial analysis of CoQtz-N at PRIME Lab used the more aggressive combustion step, but displayed less diffusive loss (relative to our analyses with Pt/Rh boats) than did CRONUS-A with that procedure, suggesting

415 variable low-temperature diffusion behavior among samples. Subsequently, internally consistent results were achieved with CoQtz-N using Pt/Rh boats, with approximately 60% lower ^{14}C concentrations than CRONUS-A. However, additional analyses of this material from this and other labs are clearly needed to work toward a consensus value.

Declaration of competing interests

420 The authors declare that they have no conflict of interest.

Acknowledgments

The authors gratefully acknowledge advice and technical assistance from Marc Caffee and Tom Woodruff of PRIME Lab. Funding for this research was provided by US National Science Foundation grant EAR-1560658 and a Purdue University Laboratory and University Core Facility Research Equipment Program grant (2017-2018).

425 **Author contributions**

This study was conceived by NL and JW. Sample preparation and analysis was done by NL and AK. NL analyzed the data and wrote the manuscript, with contributions from AK and JW.

430 **References**

Binnie, S. A., Dewald, A., Heinze, S., Voronina, E., Hein, A., Wittmann, H., Blanckenburg, F. von, Hetzel, R., Christl, M., Schaller, M., Léanni, L., Team, A., Hippe, K., Vockenhuber, C., Ivy-Ochs, S., Maden, C., Fülöp, R.-H., Fink, D., Wilcken, K. M., Fujioka, T., Fabel, D., Freeman, S. P. H. T., Xu, S., Fifield, L. K., Akçar, N., Spiegel, C., and Dunai, T. J.: Preliminary results of CoQtz-N: A quartz reference material for terrestrial in-situ cosmogenic ^{10}Be
435 and ^{26}Al measurements, Nuclear Instruments and Methods in Physics Research Section B: Beam Interactions with Materials and Atoms, 456, 203–212, https://doi.org/10.1016/j.nimb.2019.04.073, 2019.

Donahue, D. J., Jull, A. J. T., and Toolin, L.: Radiocarbon measurements at the University of Arizona AMS facility, Nuclear Instruments and Methods in Physics Research B, 52, 224–228, 1990.

Donahue, D. J., Beck, J. W., Biddulph, D., Burr, G. S., Courtney, C., Damon, P. E., Hatheway, A., Hewitt, L., Jull,
440 A. J. T., Lange, T., Lifton, N., Maddock, R., McHargue, L., O'Malley, J. M., and Toolin, L.: Status of the NSF-Arizona AMS laboratory, Nuclear Instruments and Methods in Physics Research B, 123, 51–56, 1997.

Fülöp, R., Naysmith, P., Cook, G., and Fabel, D.: Update on the performance of the SUERC *in situ* cosmogenic ^{14}C extraction line, Radiocarbon, 52, 1288–1294, 2010.

Fülöp, R. H., Wacker, L., and Dunai, T. J.: Progress report on a novel *in situ* ^{14}C extraction scheme at the University
445 of Cologne, Nuclear Inst. and Methods in Physics Research, B, 361, 20–24, https://doi.org/10.1016/j.nimb.2015.02.023, 2015.

Fülöp, R.-H., Fink, D., Yang, B., Codilean, A. T., Smith, A., Wacker, L., Levchenko, V., and Dunai, T. J.: The ANSTO – University of Wollongong in-situ ^{14}C extraction laboratory, Nuclear Inst. and Methods in Physics Research, B, 438, 207–213, https://doi.org/10.1016/j.nimb.2018.04.018, 2019.

450 Goehring, B. M., Wilson, J., and Nichols, K.: A fully automated system for the extraction of *in situ* cosmogenic carbon-14 in the Tulane University cosmogenic nuclide laboratory, Nuclear Instruments and Methods in Physics Research B, 455, 284–292, https://doi.org/10.1016/j.nimb.2019.02.006, 2019.

Hippe, K. and Lifton, N. A.: Calculating Isotope Ratios and Nuclide Concentrations for In Situ Cosmogenic ^{14}C Analyses, Radiocarbon, 56, 1167–1174, https://doi.org/10.2458/56.17917, 2014.

455 Hippe, K., Kober, F., Baur, H., Ruff, M., Wacker, L., and Wieler, R.: The current performance of the *in situ* ^{14}C extraction line at ETH, Quaternary Geochronology, 4, 493–500, https://doi.org/10.1016/j.quageo.2009.06.001, 2009.

Hippe, K., Kober, F., Wacker, L., Fahrni, S. M., Ivy-Ochs, S., Akcar, N., Schluchter, C., and Wieler, R.: An update on *in situ* cosmogenic ^{14}C analysis at ETH Zürich, Nuclear Inst. and Methods in Physics Research, B, 294, 81–86, 2013.

460 Jull, A. J. T., Scott, E. M., and Bierman, P.: The CRONUS-Earth inter-comparison for cosmogenic isotope analysis, Quaternary Geochronology, 26, 3–10, https://doi.org/10.1016/j.quageo.2013.09.003, 2015.

Lamp, J. L., Young, N. E., Koffman, T., Schimmelpfennig, I., Tuna, T., Bard, E., and Schaefer, J. M.: Update on the cosmogenic *in situ* ^{14}C laboratory at the Lamont-Doherty Earth Observatory, Nuclear Inst. and Methods in Physics Research, B, 456, 157–162, https://doi.org/10.1016/j.nimb.2019.05.064, 2019.

465 Lifton, N., Jull, A., and Quade, J.: A new extraction technique and production rate estimate for *in situ* cosmogenic ^{14}C in quartz, Geochimica Et Cosmochimica Acta, 65, 1953–1969, 2001.

Lifton, N., Goehring, B., Wilson, J., Kubley, T., and Caffee, M.: Progress in automated extraction and purification of *in situ* ^{14}C from quartz: Results from the Purdue *in situ* ^{14}C laboratory, Nuclear Inst. and Methods in Physics Research, B, 361, 381–386, https://doi.org/10.1016/j.nimb.2015.03.028, 2015.

Lupker, M., Hippe, K., Wacker, L., Steinemann, O., Tikhomirov, D., Maden, C., Haghipour, N., and Synal, H.-A.: In-situ cosmogenic ^{14}C analysis at ETH Zürich: Characterization and performance of a new extraction system, Nuclear Instruments and Methods in Physics Research Section B: Beam Interactions with Materials and Atoms, 457, 30–36, https://doi.org/10.1016/j.nimb.2019.07.028, 2019.

495   Nichols, K. A. and Goehring, B. M.: Isolation of quartz for cosmogenic *in situ* ^{14}C analysis, Geochronology, 1, 43–52, https://doi.org/10.5194/gchron-1-43-2019, 2019.

Pigati, J., Lifton, N., Jull, A. J. T., and Quade, J.: A simplified *in situ* cosmogenic ^{14}C extraction system, Radiocarbon, 52, 1236–1243, 2010.

Santos, G. M., Southon, J. R., Druffel-Rodriguez, K., Griffin, S., and Mazon, M.: Magnesium Perchlorate as an
500   Alternative Water Trap in AMS Graphite Sample Preparation: A Report on Sample Preparation at KCCAMS at the University of California, Irvine, Radiocarbon, 46, 165–174, 2004.

Schiffer, M., Stolz, A., López, D. A., Spanier, R., Herb, S., Müller-Gatermann, C., Heinze, S., Binnie, S., Melchert, J., Kivel, N., Schumann, D., Rethemeyer, J., Dunai, T., and Dewald, A.: Method developments for accelerator mass spectrometry at CologneAMS, 53Mn/3He burial dating and ultra-small $^{14}CO_2$ samples, Global and Planetary
505   Change, 184, 103053, https://doi.org/10.1016/j.gloplacha.2019.103053, 2020.

Southon, J.: Graphite reactor memory - Where is it from and how to minimize it?, Nuclear Instruments and Methods in Physics Research Section B: Beam Interactions with Materials and Atoms, 259, 288–292, 2007.

515
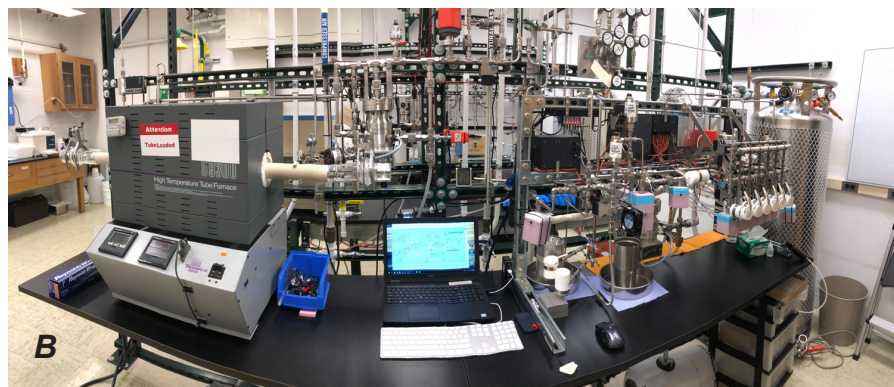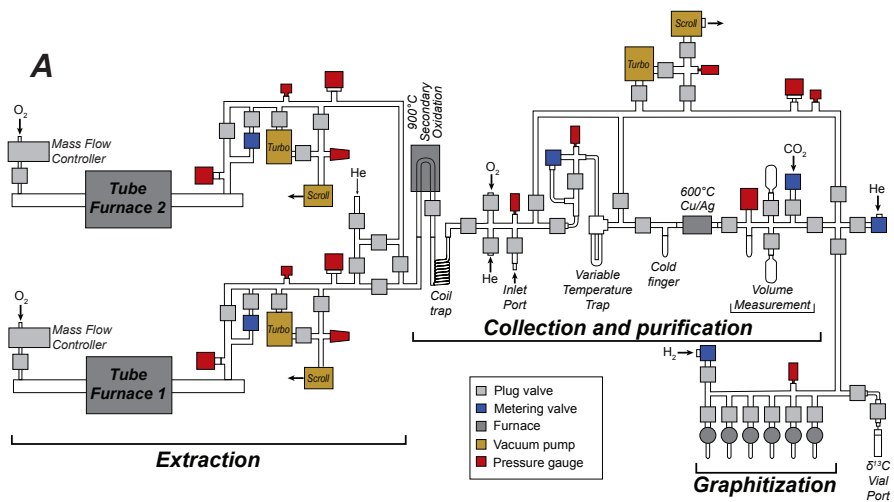
Figure 1: A) Schematic and B) photo of the Purdue Carbon Extraction and Graphitization System (PCEGS).

520

Figure 2: Compact borosilicate glass coil trap, consisting of a 9 mm o.d. x 7 mm i.d. inlet downtube (on the left), connected to a tightly coiled 6 mm o.d. x 4 mm i.d. section with subsequent outlet tube. Scale on bottom is in cm.
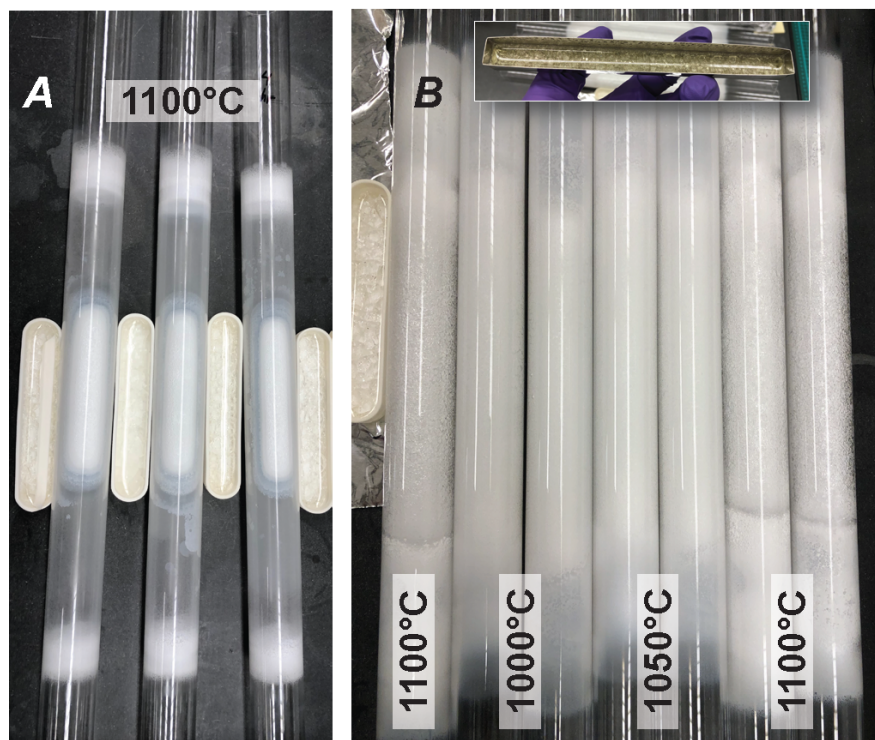
525

Figure 3: Comparison of quartz sleeve corrosion from LiBO$_2$ for A) Al$_2$O$_3$ boats and B) Pt/Rh boats (inset), after the high temperature fusion step (3 hr) at the temperatures indicated. Note the significantly greater corrosion associated with the Pt/Rh boats vs. the Al$_2$O$_3$, indicating more aggressive and uniform heating in the former, and noticeably milder corrosion from the 1050°C and 1000°C runs. The Al$_2$O$_3$ boat on the left side of B) is holding the sleeves in place but also serves as a

530

comparison to A). We speculate that the greater corrosion from LiBO$_2$ in the Pt/Rh boats reflects higher thermal conductivity of the metal boats vs. the sintered ceramic boats.

535
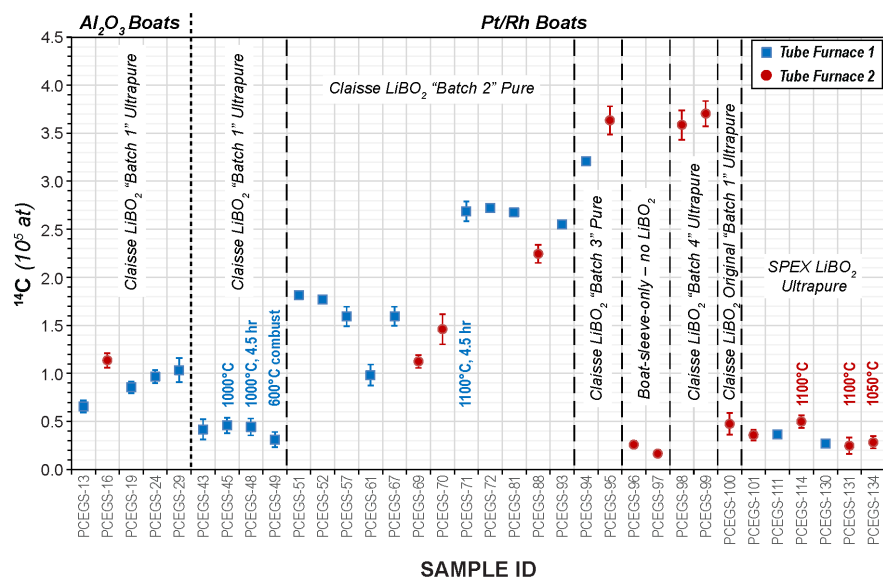
Figure 4: Procedural blank results for Al₂O₃ and Pt/Rh boats (1σ uncertainties). All blanks using Al₂O₃ boats used a 2 hr at 600°C combustion step followed by a 3 hr extraction at 1100°C (1120°C for Tube Furnace 2 due to a miscalibration at the 1100°C setpoint). All Pt/Rh Tube Furnace 1 runs were a 1 hr at 500°C combustion step followed by a 3 hr extraction step at 1100°C, except as indicated. Tube Furnace 2 combustions with Pt/Rh boats were also 1 hr at 500°C, but

540 **extractions were at 1120°C due to the miscalibration, except as indicated.**
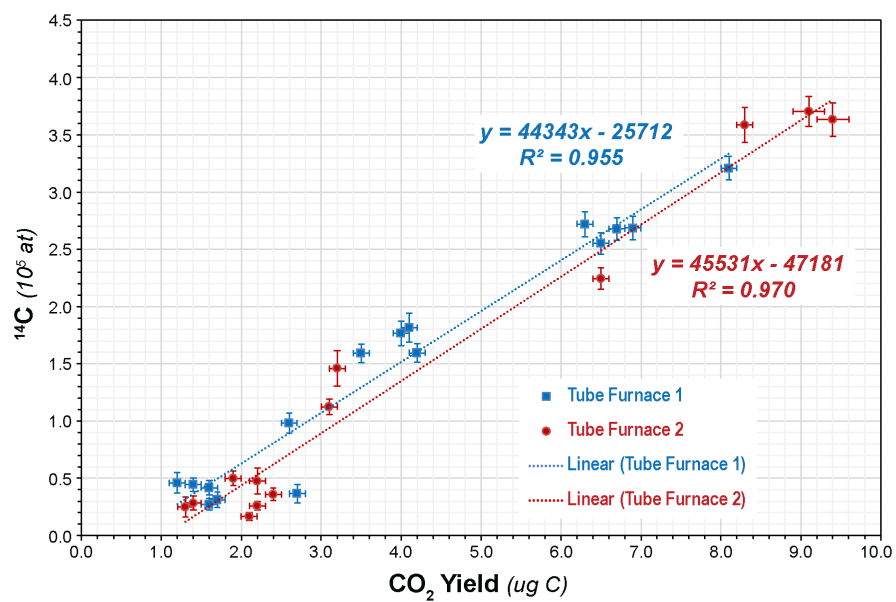
Figure 5: Linear fit between CO₂ yield in μg C vs. procedural blank in ¹⁴C atoms, for Tube Furnaces 1 and 2 (1σ uncertainties shown).

545
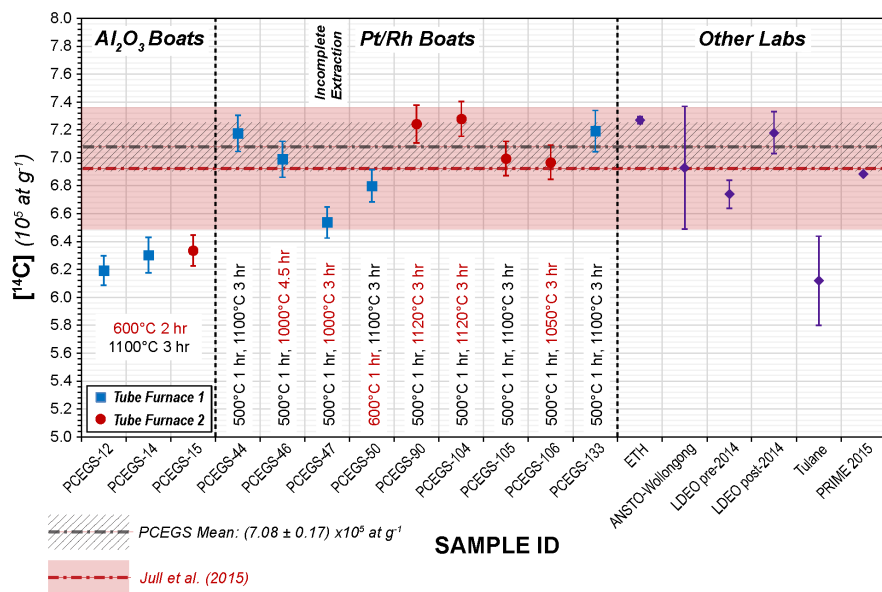
Figure 6: CRONUS-A results with experimental details (1σ uncertainties) from this study, with mean values from other studies for comparison. The PCEGS mean value includes all samples except PCEGS-47. Other labs' results: ETH (Lupker et al., 2019); ANSTO-Wollongong (Fülöp et al., 2019); LDEO (Lamp et al., 2019); Tulane (Goehring et al., 2019); PRIME 2015 (Lifton et al., 2015).

550

Table 1: Procedural flow for *in situ* [14]C extraction at PRIME Lab. See text for abbreviations

DAY 1	*DAY 2*
• Sample pretreatment – 50% v:v HNO_3 – 90 min sonication	• Flame-clean fused-silica implements. Store in laminar-flow bench
• Flame-clean fused-silica sleeve and implements. Store in laminar-flow bench	• Backfill extraction module with RP He
• Add 20 g $LiBO_2$ to sample boat	• Remove boat from furnace tube using cleaned implements. Place in laminar flow bench
• Backfill extraction module with RP He	• Remove sample from vacuum oven, cool to room temperature and add ca. 5 g to boat
• Insert sleeve into furnace tube, and boat into sleeve using cleaned implements	• Replace boat into furnace/sleeve using cleaned implements
• Evacuate extraction module to $< 5e^{-3}$ torr	• Evacuate extraction module to $< 5e^{-3}$ torr
• Add ca. 50 torr RP O_2 to furnace tube at room temperature	• Add ca. 50 torr RP O_2 to furnace tube at room temperature
• Heat furnace to extraction temperature	• Heat furnace to combustion temperature
• Hold at extraction temperature for 1 hour while bleeding O_2 through tube at resulting tube pressure (typically ca. 90 torr)	• Hold at combustion temperature for 1 hour while bleeding O_2 through tube at resulting tube pressure (typically ca. 60 torr)
• Cool furnace to <800°C to resolidify $LiBO_2$ while continuing O_2 bleed before evacuating overnight	• Evacuate extraction module to $< 5e^{-3}$ torr
• Rinse sample thoroughly in 18 MΩ water and dry in vacuum oven overnight at ca. 70°C	• Add ca. 50 torr RP O_2 to furnace tube at combustion temperature
	• Heat to furnace to extraction temperature and hold for 3 hours while evacuating CEGS module
	• Cool coil trap to -196°C with LN, then link CEGS and extraction modules, pumping only through CEGS vacuum system
	• Slowly bleed O_2 through furnace tube, secondary furnace, and coil trap to collect any evolved condensable gases, maintaining tube pressure (typically ca. 60 torr) while cooling furnace to <800°C.
	• Slowly evacuate extraction module through secondary furnace/coil trap
	• Isolate coil trap from extraction module, then transfer condensed gases to evacuated VTT with LN
	• Isolate VTT and join to MC via Cu/Ag trap.
	• Extract and purify CO_2 with VTT/Cu/Ag trap
	• Measure CO_2 yield, dilute if necessary, collect small aliquot for $\delta^{13}C$ analysis and graphitize remainder

555

Table 2: Graphitization Blanks

SAMPLE	PCEGS #	PLID[a]	Mass C μg	$^{14}C/^{13}C$ 10^{-13}	$^{14}C/C_{total}$[b] 10^{-15}
DILGAS-300	PCEGS-20	202001597	309.2 ± 3.8	1.5882 ± 0.1829	1.6709 ± 0.0019
DILGAS-300	PCEGS-21	202001598	339.6 ± 4.1	1.4773 ± 0.1817	1.5543 ± 0.0019
DILGAS-50	PCEGS-33	202100561	48.4 ± 0.6	3.7096 ± 0.4990	3.9024 ± 0.0053
DILGAS-100	PCEGS-34	202100562	92.6 ± 1.2	2.4291 ± 0.4102	2.5554 ± 0.0043
DILGAS-200	PCEGS-35	202100563	198.9 ± 2.4	1.9322 ± 0.2480	2.0326 ± 0.0026
DILGAS-500	PCEGS-36	202100564	523.5 ± 6.3	1.4752 ± 0.1897	1.5519 ± 0.0020
DILGAS-700	PCEGS-37	202100565	696.0 ± 8.4	1.4390 ± 0.2788	1.5138 ± 0.0029
DILGAS-1000	PCEGS-38	202100566	1,000.2 ± 12.1	1.4068 ± 0.1852	1.4799 ± 0.0020
DG-05072021	--	202101467	304.7 ± 3.7	2.1203 ± 0.2686	2.2305 ± 0.0028

560

Notes
a PRIME Lab ID
b δ^{13}C averages -45.6 ± 0.2 ‰$_{VPDB}$

Table 3: Al₂O₃ Procedural Blanks – all used 2 hr combustion at 600°C and 3 hr extraction at 1100°C, unless otherwise noted

565

SAMPLE	PCEGS #	PLID	C yield μg	Diluted C Mass μg	AMS C Mass μg	$\delta^{13}C$ ‰$_{VPDB}$	$^{14}C/^{13}C$ 10^{-12}	$^{14}C/C_{total}$ 10^{-14}	^{14}C 10^4 atoms
					TF1				
PB1-10012020	PCEGS-13	202001590	2.8 ± 0.1	308.2 ± 3.7	299.2 ± 3.6	-45.0 ± 0.2	0.5673 ± 0.0466	0.4256 ± 0.0494	6.5763 ± 0.7667
PB1-10272020	PCEGS-19	202001596	3.0 ± 0.1	310.4 ± 3.8	301.3 ± 3.7	-45.4 ± 0.2	0.6857 ± 0.0357	0.5502 ± 0.0379	8.5621 ± 0.5995
PB1-12032020	PCEGS-24	202100567	4.2 ± 0.1	308.6 ± 3.8	299.6 ± 3.6	-46.2 ± 0.2	0.7579 ± 0.0506	0.6252 ± 0.0534	9.6735 ± 0.8351
PB1-12152020	PCEGS-29	202100568	3.7 ± 0.1	303.8 ± 3.7	294.9 ± 3.6	-44.9 ± 0.2	0.8080 ± 0.0541	0.6784 ± 0.0572	10.3334 ± 0.8796
					TF2				
PB2-10162020[a]	PCEGS-16	202001593	4.0 ± 0.1	303.7 ± 3.7	294.8 ± 3.6	-45.2 ± 0.2	0.8731 ± 0.0460	0.7467 ± 0.0487	11.3708 ± 0.7547

Notes
All blanks here used Claisse C-0611-00, Batch C-10001 – "Batch 1" Ultrapure LiBO₂
a   1120°C extraction due to furnace miscalibration at 1100°C setpoint

570

Table 4: Pt/Rh Procedural Blanks – All used 1 hr combustion at 500°C and 3 hr extraction at 1100°C, unless otherwise noted

575

SAMPLE	PCEGS #	PLID	C Mass μg	Diluted C Mass μg	AMS C Mass μg	$\delta^{13}C$ $‰_{VPDB}$	$^{14}C/^{13}C$ 10^{-12}	$^{14}C/C_{total}$ 10^{-14}	^{14}C $10^4\ atoms$
					TF1				
PB1-02042021	PCEGS-43[g]	202100569	1.6 ± 0.1	300.8 ± 3.7	292.0 ± 3.6	-46.3 ± 0.2	0.4275 ± 0.0389	0.2768 ± 0.0412	4.1740 ± 0.6240
PB1-02092021[a]	PCEGS-45[g]	202100571	1.2 ± 0.1	300.6 ± 3.7	296.0 ± 3.6	-42.9 ± 0.2	0.4523 ± 0.0555	0.3051 ± 0.0588	4.5979 ± 0.8879
PB1-02202021[b]	PCEGS-48[g]	202100574	1.4 ± 0.1	304.1 ± 3.7	295.2 ± 3.6	-46.1 ± 0.2	0.4407 ± 0.0374	0.2912 ± 0.0397	4.4399 ± 0.6071
PB1-02232021[c]	PCEGS-49[g]	202100575	1.7 ± 0.1	304.1 ± 3.7	295.1 ± 3.6	-45.2 ± 0.2	0.3582 ± 0.0426	0.2047 ± 0.0452	3.1213 ± 0.6897
PB1-03232021	PCEGS-51[h]	202101468	4.1 ± 0.1	315.8 ± 3.8	306.5 ± 3.7	-43.8 ± 0.2	1.2488 ± 0.0737	1.1467 ± 0.0779	18.1577 ± 1.2520
PB1-03252021	PCEGS-52[h]	202101469	4.0 ± 0.1	307.8 ± 3.7	298.8 ± 3.6	-44.6 ± 0.2	1.2531 ± 0.0644	1.1446 ± 0.0680	17.6652 ± 1.0711
PB1-04062021	PCEGS-57[h]	202101474	3.5 ± 0.1	304.2 ± 3.7	295.3 ± 3.6	-43.9 ± 0.2	1.1538 ± 0.0484	1.0438 ± 0.0513	15.9198 ± 0.8064
PB1-04152021	PCEGS-61[h]	202101478	2.6 ± 0.1	305.1 ± 3.7	296.2 ± 3.6	-44.4 ± 0.2	0.7731 ± 0.0535	0.6423 ± 0.0566	9.8250 ± 0.8742
PB1-04292021	PCEGS-67[h]	202101479	4.2 ± 0.1	307.8 ± 3.7	298.8 ± 3.6	-44.4 ± 0.2	1.1447 ± 0.0466	1.0340 ± 0.0493	15.9575 ± 0.7850
PB1-05252021[d]	PCEGS-71[h]	202101639	6.9 ± 0.1	316.7 ± 3.9	307.4 ± 3.7	-44.8 ± 0.2	1.7682 ± 0.0572	1.6911 ± 0.0605	26.8532 ± 1.0157
PB1-06012021	PCEGS-72[h]	202101640	6.3 ± 0.1	311.8 ± 3.8	302.7 ± 3.7	-45.7 ± 0.2	1.8171 ± 0.0637	1.7401 ± 0.0672	27.2047 ± 1.1013
PB1-06192021	PCEGS-81[h]	202101649	6.7 ± 0.1	308.5 ± 3.8	299.4 ± 3.6	-42.3 ± 0.2	1.8025 ± 0.0573	1.7310 ± 0.0607	26.7745 ± 0.9950
PB1-07242021	PCEGS-93[h]	202101661	6.5 ± 0.1	306.9 ± 3.7	297.9 ± 3.6	-45.2 ± 0.2	1.7384 ± 0.0544	1.6577 ± 0.0575	25.5091 ± 0.9372
PB1-08062021	PCEGS-94[i]	202101662	8.1 ± 0.1	310.3 ± 3.8	301.2 ± 3.7	-44.7 ± 0.2	2.1215 ± 0.0576	2.0626 ± 0.0608	32.0902 ± 1.0248
PB1-10222021	PCEGS-111[k]	202102037	2.7 ± 0.1	305.0 ± 3.7	296.0 ± 3.6	-45.1 ± 0.2	0.3905 ± 0.0514	0.2389 ± 0.0544	3.6539 ± 0.8329
PB1-11192021	PCEGS-130[k]	202102056	1.6 ± 0.1	302.1 ± 3.7	293.2 ± 3.6	-45.8 ± 0.2	0.3348 ± 0.0320	0.1796 ± 0.0341	2.7205 ± 0.5175
					TF2				
PB2-05112021[e]	PCEGS-69[h]	202101637	3.1 ± 0.1	309.1 ± 3.8	300.1 ± 3.7	-44.6 ± 0.2	0.8523 ± 0.0405	0.7260 ± 0.0429	11.2509 ± 0.6798
PB2-05132021[e]	PCEGS-70[h]	202101638	3.2 ± 0.1	307.2 ± 3.7	298.2 ± 3.6	-42.6 ± 0.2	1.0608 ± 0.0951	0.9477 ± 0.1005	14.5966 ± 1.5576
PB2-07142021[e]	PCEGS-88[h]	202101656	6.5 ± 0.1	304.3 ± 3.7	295.4 ± 3.6	-45.5 ± 0.2	1.5619 ± 0.0557	1.4711 ± 0.0588	22.4454 ± 0.9380
PB2-08112021[e]	PCEGS-95[i]	202101663	9.4 ± 0.2	304.9 ± 3.7	295.9 ± 3.6	-45.3 ± 0.2	2.4222 ± 0.0865	2.3766 ± 0.0912	36.3332 ± 1.4618
Boat-HCl[e]	PCEGS-96	202101663	2.2 ± 0.1	305.2 ± 3.7	296.2 ± 3.6	-45.8 ± 0.2	0.3249 ± 0.0228	0.1697 ± 0.0246	2.5962 ± 0.3770
Boat- HNO₃[e]	PCEGS-97	202101669	2.1 ± 0.1	304.9 ± 3.7	296.0 ± 3.6	-45.1 ± 0.2	0.2671 ± 0.0226	0.1091 ± 0.0244	1.6671 ± 0.3729
PB2-08312021[e]	PCEGS-98[i]	202101670	8.3 ± 0.1	307.3 ± 3.7	298.3 ± 3.6	-45.9 ± 0.2	2.3763 ± 0.0903	2.3272 ± 0.0951	35.8579 ± 1.5277
PB2-09022021[e]	PCEGS-99[i]	202102024	9.1 ± 0.2	303.4 ± 3.7	294.5 ± 3.6	-45.0 ± 0.2	2.4769 ± 0.0767	2.4350 ± 0.0809	37.0417 ± 1.3107
PB2-09082021[e]	PCEGS-100[g]	202102025	2.2 ± 0.1	306.0 ± 3.7	297.0 ± 3.6	-43.9 ± 0.2	0.4575 ± 0.0692	0.3102 ± 0.0732	4.7589 ± 1.1240
PB2-09282021[e]	PCEGS-101[k]	202102026	2.4 ± 0.1	313.1 ± 3.8	303.9 ± 3.7	-44.6 ± 0.2	0.3796 ± 0.0328	0.2287 ± 0.0350	3.5907 ± 0.5509
PB2-10262021	PCEGS-114[k]	202102027	1.9 ± 0.1	302.2 ± 3.7	293.3 ± 3.6	-45.4 ± 0.2	0.4763 ± 0.0398	0.3287 ± 0.0422	4.9805 ± 0.6425
PB2-11232021	PCEGS-131[k]	202102057	1.3 ± 0.1	304.4 ± 3.7	295.5 ± 3.6	-45.6 ± 0.2	0.3183 ± 0.0541	0.1627 ± 0.0572	2.4830 ± 0.8728
PB2-12022021[f]	PCEGS-134[k]	202102060	1.4 ± 0.1	301.9 ± 3.7	293.0 ± 3.6	-45.9 ± 0.2	0.3420 ± 0.0394	0.1871 ± 0.0417	2.8326 ± 0.6326

Notes

a   1000°C extraction, 3 hr

580   b   1000°C extraction, 4.5 hr
      c   600°C combustion, 1 hr
      d   1100°C extraction, 4.5 hr
      e   1120°C extraction due to furnace miscalibration at 1100°C setpoint
      f   1050°C extraction
585   g   Claisse C-0611-00, Batch C-10001 – "Batch 1" Ultrapure
      h   Claisse C-0610-00, Batch C-17000-10 – "Batch 2" Pure
      i   Claisse C-0610-00, Batch C-19000-10 – "Batch 3" Pure
      j   Claisse C-0611-00, Batch C-19001-10 – "Batch 4" Ultrapure
      k   SPEX Certi-Prep FFB-0000-03, Lot 240920D-2904 Ultrapure
590

Table 5: Intercomparison samples – All analyses used 1 hr combustion at 500°C and 3 hr extraction at 1100°C, unless otherwise noted

SAMPLE	PCEGS #	PLID	Mass Quartz g	C yield μg	Diluted mass C μg	AMS Split Mass C μg	$\delta^{13}C$ $\permil_{VPDB}$	$^{14}C/^{13}C$ 10^{-11}	$^{14}C/C_{total}$ 10^{-13}	^{14}C 10^{6} at	$[^{14}C]$ 10^{5} atoms g^{-1}	^{14}C Blank 10^{4} atoms
							CRONUS-A					
							Al$_2$O$_3$					
CRA-09172020[a]	PCEGS-12	202001589	5.0549	24.7 ± 0.3	306.4 ± 3.7	297.4 ± 3.6	-41.6 ± 0.2	1.9916 ± 0.0210	2.0868 ± 0.0222	3.1303 ± 0.0535	6.1925 ± 0.1058	7.5692 ± 1.4042
CRA-10072020[a]	PCEGS-14	202001591	5.0008	25.5 ± 0.4	377.6 ± 4.6	366.5 ± 4.4	-42.9 ± 0.2	1.6313 ± 0.0242	1.7048 ± 0.0256	3.1519 ± 0.0639	6.3028 ± 0.1279	7.5692 ± 1.4042
CRA-10132020[a]	PCEGS-15	202001592	5.0556	25.7 ± 0.4	303.2 ± 3.7	294.3 ± 3.6	-42.2 ± 0.2	2.0829 ± 0.0239	2.1819 ± 0.0252	3.2033 ± 0.0562	6.3361 ± 0.1113	11.3708 ± 0.7547
							Pt/Rh					
CRA-02062021	PCEGS-44	202100570	5.0415	26.3 ± 0.4	303.0 ± 3.7	294.1 ± 3.6	-43.1 ± 0.2	2.3000 ± 0.0297	2.4085 ± 0.0313	3.6174 ± 0.0656	7.1753 ± 0.1300	4.1740 ± 0.6240
CRA-02112021[b]	PCEGS-46	202100572	5.0099	26.2 ± 0.4	302.4 ± 3.7	293.5 ± 3.6	-42.1 ± 0.2	2.2316 ± 0.0296	2.3390 ± 0.0313	3.5020 ± 0.0649	6.9902 ± 0.1295	4.4399 ± 0.8879
CRA-02182021[c]	PCEGS-47	202100573	5.0048	25.3 ± 0.4	303.9 ± 3.7	295.0 ± 3.6	-43.4 ± 0.2	2.0817 ± 0.0236	2.1776 ± 0.0249	3.2722 ± 0.0558	6.5381 ± 0.1115	4.5979 ± 0.6071
CRA-02252021[d]	PCEGS-50	202100576	5.0630	23.1 ± 0.3	302.4 ± 3.7	293.5 ± 3.6	-42.0 ± 0.2	2.1861 ± 0.0251	2.2910 ± 0.0265	3.4425 ± 0.0589	6.7993 ± 0.1163	3.1213 ± 0.6897
CRA-07172021[e]	PCEGS-90	202101658	5.0250	30.3 ± 0.4	309.6 ± 3.8	300.5 ± 3.7	-42.6 ± 0.2	2.3751 ± 0.0296	2.4891 ± 0.0312	3.6395 ± 0.0685	7.2428 ± 0.1362	22.4454 ± 0.9380
CRA-10072021[e]	PCEGS-104	202102030	5.0568	25.9 ± 0.4	303.5 ± 3.7	294.6 ± 3.6	-42.9 ± 0.2	2.3318 ± 0.0268	2.4425 ± 0.0283	3.6810 ± 0.0628	7.2793 ± 0.1241	3.5907 ± 0.5509
CRA-10092021	PCEGS-105	202102031	4.7910	24.9 ± 0.3	304.5 ± 3.7	295.6 ± 3.6	-43.0 ± 0.2	2.1205 ± 0.0240	2.2197 ± 0.0253	3.3516 ± 0.0591	6.9955 ± 0.1234	3.7317 ± 1.7660
CRA-10122021[f]	PCEGS-106	202102032	4.7458	25.2 ± 0.4	306.0 ± 3.7	297.0 ± 3.6	-43.1 ± 0.2	2.0775 ± 0.0261	2.1740 ± 0.0275	3.3071 ± 0.0587	6.9686 ± 0.1237	2.8326 ± 0.6326
CRA-12012021	PCEGS-133	202102059	5.0281	25.3 ± 0.4	303.2 ± 3.7	294.3 ± 3.6	-43.8 ± 0.2	2.2933 ± 0.0369	2.3997 ± 0.0389	3.6163 ± 0.0743	7.1922 ± 0.1477	3.1872 ± 0.6600
							CoQtz-N					
							Al$_2$O$_3$					
CQN-10222020[a]	PCEGS-18	202001595	5.0112	7.5 ± 0.1	307.2 ± 3.7	298.2 ± 3.6	-44.6 ± 0.2	0.8281 ± 0.0133	0.8549 ± 0.0140	1.2412 ± 0.0303	2.4768 ± 0.0604	7.5692 ± 1.4042
							Pt/Rh					
CQN-05012021	PCEGS-68	202101480	5.0525	7.0 ± 0.1	307.9 ± 3.7	298.8 ± 3.6	-43.6 ± 0.2	0.9122 ± 0.0134	0.9444 ± 0.0142	1.3071 ± 0.0419	2.5870 ± 0.0830	15.1188 ± 3.1330
CQN-10052021[e]	PCEGS-103	202102029	5.0289	6.2 ± 0.1	304.7 ± 3.7	295.7 ± 3.6	-45.3 ± 0.2	0.8673 ± 0.0164	0.8954 ± 0.0173	1.3321 ± 0.0317	2.6488 ± 0.0630	3.5907 ± 0.5509

Notes
a   2 hr at 600°C combustion
b   4.5 hr at 1000°C extraction
c   3 hr at 1000°C extraction
d   1 hr at 600°C combustion
e   3 hr at 1120°C extraction
f   3 hr at 1050°C extraction